Vector magnetometry of Fe/Cr/Fe trilayers with biquadratic coupling

R Mansell,* D Petit, A Fernández-Pacheco, JH Lee, S-L Chin, R Lavrijsen, and R P Cowburn
Cavendish Laboratory, University of Cambridge, JJ Thomson Avenue, Cambridge CB3 0HE, UK

The magnetic reversal of epitaxial Fe / Cr / Fe trilayer samples grown on GaAs is studied. In wedged samples both long and short period coupling oscillations associated with Ruderman-Kittel-Kasuya-Yosida (RKKY) coupling in Cr are seen in the easy axis saturation fields. By using vector vibrating sample magnetometry and both longitudinal and transverse magneto-optical Kerr effect magnetometry we are able to determine the exact reversal path of both the magnetic layers. Changes in the reversal behavior are seen with sub-monolayer changes of the thickness of the Cr interlayer. The two main reversal paths are described in terms of whether the reversal is dominated by bilinear RKKY coupling, which leads to an antiparallel state at remanence or by biquadratic coupling which leads to a 90 degree alignment of layers at remanence. The changing reversal behaviour is discussed with respect to the possibility of using such systems for multilayer memory applications and, in particular, the limits on the required accuracy of the sample growth.

INTRODUCTION

In multilayer systems with Ruderman-Kittel-Kasuya-Yosida (RKKY) coupling[1,2]complex transitions depending on the strength of the coupling and direction of the applied field are possible[3,4]. This is particularly important in systems with four-fold anisotropy where there is often a large biquadratic coupling term, which favours the alignment of the magnetization in coupled layers at 90 degrees to each other[4–6]. One widely studied system[7–14] with four-fold anisotropy, and pronounced biquadratic coupling, is that of Fe/Cr. Several different origins of biquadratic coupling have been proposed. There are intrinsic mechanisms, where the biquadratic is associated with higher harmonics of the exchange coupling[15], as well as several extrinsic mechanisms. For Cr, which has an antiferromagnetic structure, the RKKY strength can oscillate in a layer-by-layer manner. It has been suggested that monolayer steps can then lead to a favorable 90 degree alignment between coupled layers[16]. Another suggestion is that of 'loose spins' where magnetic atoms in the spacer layer or weakly coupled at the interface give rise to the biquadratic coupling[17]. Further, it has been proposed that the dipole coupling at a rough interface can also cause an effective biquadratic term[6]. Various studies have looked at the biquadratic coupling in Fe/Cr multilayers[5,9,18], and experimental data has been found to support the different theories[19].

One emerging area of interest for coupled multilayer samples, where the details of the magnetic reversal are important, is in three-dimensional memory devices[20–24]. By carefully tuning the interlayer coupling designed magnetic states can be achieved that allow multiple bits to be stored in a multilayer[24] or even propagated through the stack[20,21]. These applications require precise control of both the anisotropy of the system as well as the interlayer coupling[20,25]. Epitaxial samples provide the opportunity to gain precise control over the anisotropy which can be propagated over many repeats of a multilayer sample. Control over interlayer coupling is provided through the RKKY mechanism, which allows a wide range of coupling strengths to be accessed.

In this paper the complex reversal of coupled Fe layers with four-fold anisotropy and significant biquadratic coupling is studied as a function of Cr interlayer thickness. By using vector magnetometry techniques, aided by the use of magnetic layers with asymmetric thicknesses, we are able to determine the precise switching of a trilayer system. These results are discussed in terms of the possibilities for creating multilayer structures for logic and memory applications and the limits on the growth required for this materials system.

SAMPLE GROWTH

A series of epitaxial Fe/Cr/Fe(001) trilayers were grown, where the Cr was either in the form of a wedge or took a single thickness value. The samples were grown on GaAs(001) substrates by molecular beam epitaxy with direct electron beam sources in a chamber with a base pressure of 2×10^{-10} mbar. The GaAs surface oxide was removed by heating the substrates in a buffer chamber to 600 °C for one hour. Data from three samples are shown in this paper. Two samples have an interlayer wedge of Cr from 0 nm to 4 nm grown using a linear shutter, with the thickness increasing along the Fe magnetic hard axis, whilst the third has a Cr interlayer with a fixed thickness of nominally 3.0 nm. For one Cr wedge sample and the fixed thickness Cr interlayer, an initial buffer layer of 1.5 nm of Fe was grown at 150 °C, which helps promote the epitaxy of the following layers. This is followed by a 90 nm Ag / 15 nm Cr buffer also grown at 150 °C which was then annealed at 300 °C for one hour in order to increase the terrace width of the surface before Fe/Cr growth[10]. The Fe/Cr trilayers were grown at 100 °C with the first 4nm thick Fe layer, followed by either a wedge or single thickness of Cr, then a 2 nm thick Fe layer. The second wedge sample was grown using a 20 nm Fe / 15 nm Cr buffer layer grown at 150 °C and annealed at 300 °C for one hour, with Fe/Cr trilayer growth at 150 °C[10]. The trilayers were finally capped with Cr. The results do not appear to be strongly dependent on the buffer layers or

growth temperature used. The growth was monitored by in-situ RHEED which showed streaky patterns for all the layers indicating 2D-like surfaces. The layers were then removed from the chamber to be magnetically characterized.

VECTOR MOKE MEASUREMENTS

The magnetic easy axes of the Fe layers lie along the [100] and [010] direction of the GaAs substrate[7]. In figure 1(a) the easy axis saturation field measured by the magneto optical Kerr effect (MOKE) of a sample grown with a Fe/Ag/Cr buffer and a Cr wedge from 0 nm to 4.5 nm is shown as a function of the Cr thickness. The easy axis saturation field is a function of the RKKY coupling – the stronger the coupling the harder it is to align the two layers to the applied field. The first two long wavelength antiferromagnetic peaks are seen at around 7 ML and 20 ML (1.0 nm and 2.9 nm, respectively), corresponding to the maxima in the saturation field[13]. The short wavelength fluctuations in coupling strength commonly seen in Cr are also clearly visible[12]. Since Cr is itself antiferromagnetic, odd numbers of monolayers increase the antiferromagnetic coupling strength whilst an even number of monolayers leads to a reduction[26]. A close up of the second antiferromagnetic peak around 20 ML is shown in figure 2(b). This is from the sample with a Fe/Cr buffer, however, the similarity with the data in figure 1(a) shows the reproducibility of the magnetic behaviour even with the different buffer layers. The labelled points correspond to the easy axis hysteresis loops shown in figure 2. This region is of greatest interest for well controlled switching for data storage and memory applications[20,27] due to the balance between the anisotropy of the Fe layers (around 550 Oe) and the RKKY coupling strength for a layer thicknesses up to a few nanometres.

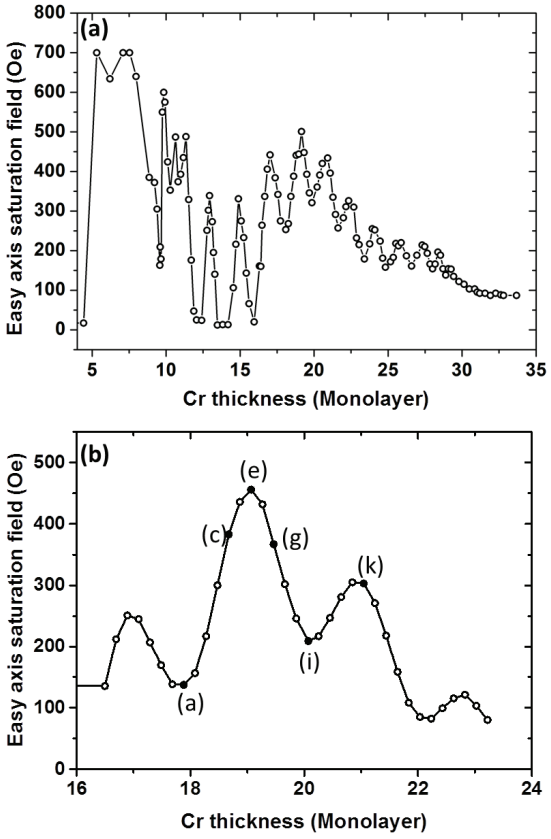

FIG. 1. (a) Easy axis saturation field as a function of Cr interlayer thickness for a Fe / Ag / Cr / 4 nm Fe / Cr wedge / 2 nm Fe sample. (b) Data around the second long-wavelength antiferromagnetic peak on a Fe / Cr / 4 nm Fe / Cr wedge / 2 nm Fe sample. The marked data points correspond to MOKE hysteresis loops given in figure 2.

In figure 2 the left hand column gives easy axis longitudinal MOKE signals for a series of positions as marked in figure 1(b), with the right-hand column giving the simultaneously measured transverse MOKE signal. The combination of the longitudinal and transverse signals gives much more information than just the longitudinal MOKE. Due to the four-fold anisotropy strong transverse signals occur when the magnetizations of the layers lies perpendicular to the field direction. Whilst MOKE in multilayer systems is very sensitive to the exact optical transitions and so exact assignment of the magnetic state of the sample is not straightforward[20,28], this information allows trends in magnetic behaviour to be tracked across changing Cr thickness. Starting from a minimum in energy around 18 ML (figure 2(a, b))[29] we see a complex reversal with five states present in the major loop. Both the longitudinal (figure 2(a)) and transverse MOKE (figure 2(b)) show significant signals at zero applied field suggesting that a non-collinear state is reached. Figures 2(c) and 2(d) show the MOKE signals slightly below the peak of the coupling, and whilst the features are similar to those in figures 2(a) and 2(b), they have become less well-defined. At around 19 ML, the peak in the coupling strength, the loops have changed significantly (figures 2(e) and 2(f)). A near-zero remanent state has appeared in both the longitudinal and transverse directions. This suggests that the coupling is strong enough to achieve an anti-parallel state at remanence. The increased noise in the normalized transverse loop suggests a reduced transverse signal, consistent with an antiparallel state. The slightly non-zero remanence is likely due to two competing effects. Firstly, the two layers are of different thickness, and, secondly, the depth dependence of the MOKE, lead here to a non-compensating signal. Figures 2(g) and 2(h) show lower coupling with increased Cr thickness compared to the previous panel, seen by the reduced saturation field. Whilst the total coupling, as measured by the saturation field, is similar to that of 2(c), the loop is different and has a near zero magnetization remanent state. This suggests that the relative contribution of the bilinear and biquadratic RKKY terms has changed leading to dominance of the bilinear term. However, a transition in the transverse MOKE has also appeared.

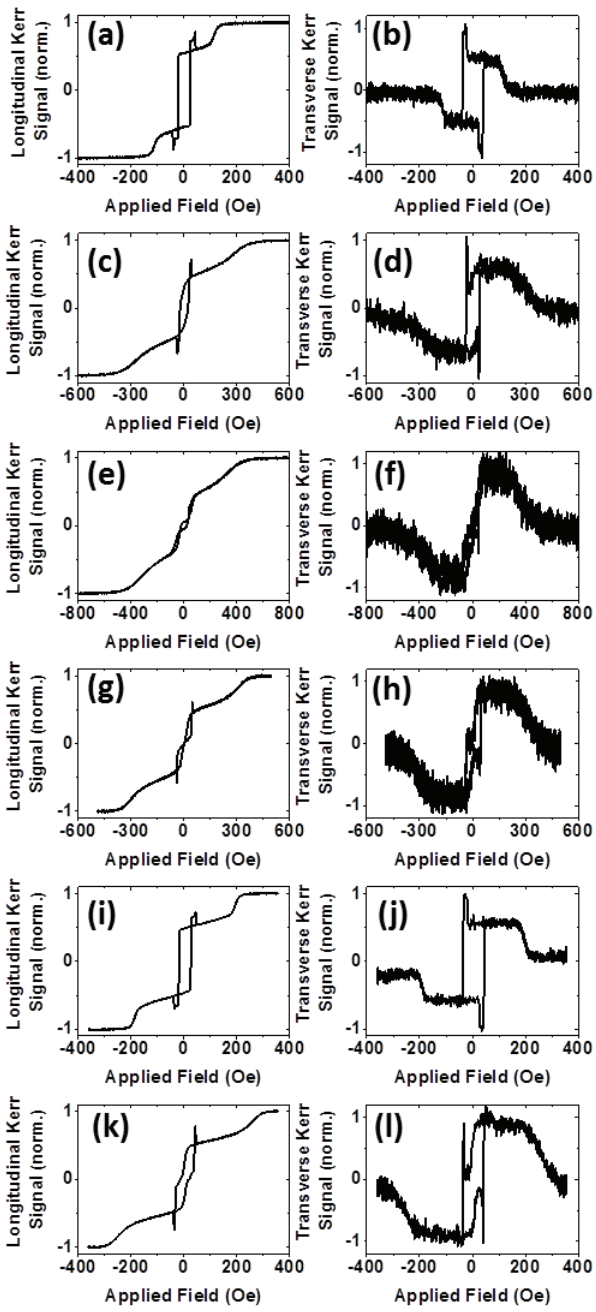

FIG. 2. (a) The longitudinal and (b) transverse MOKE around 18 ML Cr interlayer thickness. (c) Longitudinal and (d) transverse MOKE around 18.7 ML Cr interlayer thickness. (e) Longitudinal and (f) transverse MOKE around 19 ML Cr interlayer thickness. (g) Longitudinal and (h) transverse MOKE around 19.4 ML Cr interlayer thickness. (i) Longitudinal and (j) transverse MOKE around 20 ML Cr interlayer thickness. (k) Longitudinal and (l) transverse MOKE around 21 ML Cr interlayer thickness. The data is taken from a Fe / Cr / Fe 4 nm / Cr / Fe 2 nm trilayer. The saturation fields taken from the longitudinal MOKE data (a,c,e,g,i,k) are marked in figure 1.

At the minimum of coupling at 20 ML in figures 2(i) and 2(j) there is again a similar state to that found at 18 ML. At the next peak in coupling at around 21 ML (figures 2(k) and 2(l)), there is a loop which combines features of the previous two positions. An apparent antiparallel state is found, but it does not occur at remanence but at slightly greater fields. This is consistent with there being less bilinear coupling at this peak than at 19 ML as would be expected from the reduced saturation field.

VECTOR VSM MEASUREMENTS

To provide clearer assignment of the transitions seen in figures 2(a) and 2(b) or 2(i) and 2(j) a sample with a fixed, nominally 3.0 nm (21 ML), Cr interlayer thickness grown on a Fe/Ag/Cr buffer is studied. It shows very similar transitions to those seen in MOKE, however the single Cr thickness allows measurement by VSM where an accurate assignment of the magnetic configurations can be made. This data is shown in figure 3(a) for the VSM signal parallel to the applied field and 3(b) for the signal perpendicular to the applied field, equivalent to the longitudinal and transverse MOKE, respectively. The dotted horizontal lines give the positions of one-third and two-thirds of the total signal, the most likely values for the magnetization given the magnetic layer thicknesses of 4 nm and 2 nm. The data is normalized to the saturation magnetization of the sample, with the black and red arrows showing the magnetic configuration of the two layers. The first transition coming from saturation (configuration (i) to (ii)) is now much more coercive than in the MOKE loop, although this could be due to variations in the coupling across the sample or that transitions in wedged samples may be driven by domain wall nucleation events at different coupling strengths to that being measured[30]. By comparing the longitudinal and transverse signals we can accurately assign the transitions. The first transition from saturation is due to the 2 nm layer rotating 90 degrees, which matches the observed configuration of a longitudinal component around two-thirds of the saturated value and a transverse signal to be around one-third of the saturated value (configuration (ii)). It is noticeable that the longitudinal signal is slightly larger, and the transverse signal slightly lower than the expected value. This is consistent with the two layers canting towards the applied field and the canting reduces, at least in the longitudinal direction, as the field is reduced. In four-fold systems with bilinear coupling it is possible for such a 90 degree state to be the minimum energy state even without the addition of biquadratic coupling under certain applied field conditions[3]. The next transition (configuration (ii) to (iii)) is due to a rotation of both layers. The normalized magnetizations show that, unusually, two-thirds of the magnetization is pointing in the transverse direction with only one third along the applied field. This magnetization data means that both the thicker and thinner layer have rotated 90 degrees during the transition (configuration (iii)). This

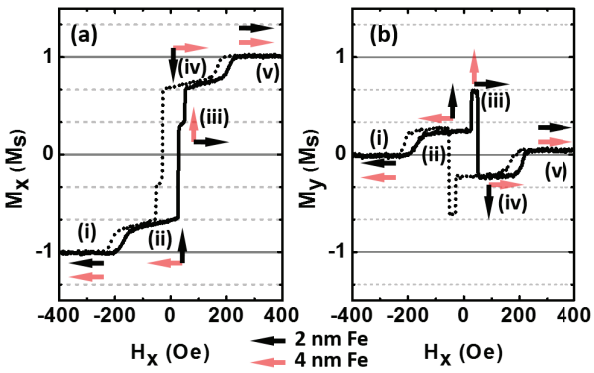

FIG. 3. (a) Magnetization measured by vibrating sample magnetometry (a) parallel to the applied field and (b) transverse to the applied field. The arrows show the directions of the two Fe layers determined from the data. The sample consists of 4 nm Fe / 3 nm Cr / 2 nm Fe grown on an Fe/Ag/Cr buffer.

retains the energy minimum of 90 degree coupling, due to a biquadratic RKKY term, whilst decreasing the Zeeman energy term by turning the thinner layer into the field direction. This configuration is not particularly stable with increasing field, however. The next transition is also due to a 90 degree rotation of both layers, with the thicker layer rotating into the field direction and the thinner layer rotating away from the field direction (configuration (iv)). This gives the increase in moment along the applied field and the partial reversal of the moment along the direction transverse to the field. It can be seen that this state is the same as that found on reducing the field from positive saturation. Again, the 90 degrees between neighbouring layers is maintained but a significant amount of Zeeman energy is gained by turning the thicker layer to the applied field direction. The existence of the three transitions in the major loop which maintain the 90 degree coupling is good evidence for the reversal being dominated by biquadratic coupling. This reversal pattern is also seen at the minima in coupling where the bilinear term is weakest, consistent with the biquadratic coupling playing an important role. The behaviour is quite distinct from that found in four-fold anisotropy systems with only bilinear RKKY coupling[3].

DISCUSSION

The VSM data can also be used to understand the behaviour of other reversal paths seen in figure 2. In particular, we study the reversal path of the position with the highest saturation field whose data is reproduced in figure 4 now with arrows marking the most likely reversal path. From negative saturation (i) there is a smeared transition to a plateau at position (ii). This position also has the maximum transverse signal. Consistent with the VSM data this first transition is therefore a rotation of the top 2 nm layer by 90 degrees. The second transition occurs just before zero field and leads to very little signal in either longitudinal or transverse Kerr data (iii). This is likely an antiparallel state as would be expected at remanence in a sytem with strong antiferromagnetic coupling. There is a small transition just after saturation (iv), which is likely the joint reversal of both layers. This leads to the thicker layer pointing into the field direction, which lowers the Zeeman energy, whilst preserving the antiparallel alignment. At higher fields the thinner 2 nm Fe layer again rotates by 90 degrees (v) before turning into the field direction (vi). It is notable how little hysteresis occurs in this reversal, consistent with a high coupling to anisotropy ratio[3].

An important conclusion from this data is that there is a very distinct change in reversal behaviour and remanent state with submonolayer changes in Cr thickness. For the multilayer memory and logic applications that motivate this research, it is a requirement that the coupling is reproduced over the whole stack, which could be tens of layers thick. The data presented here shows that, in order to achieve reproducible coupling in this system, the interlayers need to be grown with a thickness variation of less than half a monolayer. This is difficult to achieve since RHEED oscillation tend not to persist to such thick layers and the ability of other in-situ thickness measuring techniques such as quartz crystals is only accurate to around 5 % of the total thickness. This suggests that if four-fold multilayer systems are useful for these applications then interlayers which do not show layer by layer oscillation and, preferably, only have small biquadratic terms, would be more suitable. This work shows, however, the importance of vector magnetometry in allowing the exact reversal mechanism of the layers to

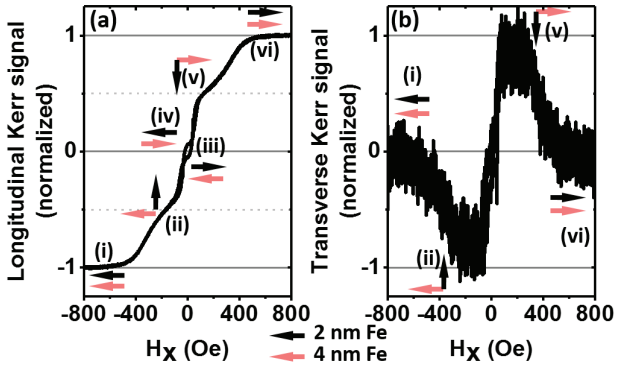

FIG. 4. (a) Longitudinal and (b) transverse MOKE data (the same as figure 2(e) and 2(f)) on a Fe / Cr / Fe 4 nm / Cr / Fe 2 nm trilayer with arrows to show the suggested magnetic configuration during the major loop.

be determined under the complex conditions of four-fold anisotropy with bilinear and biquadratic coupling.

CONCLUSION

A series of Fe 4 nm / Cr / Fe 2 nm trilayers were grown with either wedged or fixed thickness Cr interlayers, showing monolayer variation in the coupling strength. By using both MOKE and VSM vector magnetometry two distinct reversal paths were shown around the second antiferromagnetic peak. One state leads to an antiparallel alignment of the two layers at remanence, whilst the other leads to a 90 degree state. The unusual loop found at lower couping strength requires vector magnetometry to determine its complex reversal path. This approach allows the suitability of such structures for multilayer memory application to be explored and shows what level of reproducibility in coupling strength is required in large multilayer stacks for possible applications in magnetic logic and memory.

ACKNOWLEDGEMENTS

This research is funded by the European Community under the Seventh Framework Program ERC Contract No. 247368: 3SPIN and the Netherlands Organization for Scientific Research (NWO-680-50-1024 and NWO-680-47-428). A.F.-P. acknowledges support from the EPSRC Early Career Fellowship EP/M008517/1 and a Winton Fellowship.

REFERENCES

* rhodri.mansell@aalto.fi

[1] P. Bruno and C. Chappert, Phys. Rev. Lett. **67**, 1602 (1991).
[2] P. Bruno and C. Chappert, Phys. Rev. B **46**, 261 (1992).
[3] B. Dieny and J. P. Gavigan, Journal of Physics: Condensed Matter **2**, 187 (1990).
[4] J. Meersschaut, C. L'abbé, F. M. Almeida, J. S. Jiang, J. Pearson, U. Welp, M. Gierlings, H. Maletta, and S. D. Bader, Phys. Rev. B **73**, 144428 (2006).
[5] A. J. R. Ives, J. A. C. Bland, R. J. Hicken, and C. Daboo, Phys. Rev. B **55**, 12428 (1997).
[6] S. Demokritov, E. Tsymbal, P. Grünberg, W. Zinn, and I. K. Schuller, Phys. Rev. B **49**, 720 (1994).
[7] G. Wastlbauer and J. A. C. Bland, Advances in Physics **54**, 137 (2005).
[8] M. Grimsditch, S. Kumar, and E. E. Fullerton, Phys. Rev. B **54**, 3385 (1996).
[9] E. E. Fullerton, K. T. Riggs, C. H. Sowers, S. D. Bader, and A. Berger, Phys. Rev. Lett. **75**, 330 (1995).
[10] C. M. Schmidt, D. E. Bürgler, D. M. Schaller, F. Meisinger, and H.-J. Güntherodt, Phys. Rev. B **60**, 4158 (1999).
[11] R. W. Wang, D. L. Mills, E. E. Fullerton, J. E. Mattson, and S. D. Bader, Phys. Rev. Lett. **72**, 920 (1994).
[12] J. Unguris, R. J. Celotta, and D. T. Pierce, Phys. Rev. Lett. **67**, 140 (1991).
[13] S. S. P. Parkin, N. More, and K. P. Roche, Phys. Rev. Lett. **64**, 2304 (1990).
[14] M. N. Baibich, J. M. Broto, A. Fert, F. N. Van Dau, F. Petroff, P. Etienne, G. Creuzet, A. Friederich, and J. Chazelas, Phys. Rev. Lett. **61**, 2472 (1988).
[15] D. Edwards, J. Ward, and J. Mathon, Journal of Magnetism and Magnetic Materials **126**, 380 (1993).
[16] J. C. Slonczewski, Phys. Rev. Lett. **67**, 3172 (1991).
[17] J. C. Slonczewski, Journal of Applied Physics **73**, 5957 (1993).
[18] A. Fuss, S. Demokritov, P. Grünberg, and W. Zinn, Journal of Magnetism and Magnetic Materials **103**, L221 (1992).
[19] S. O. Demokritov, Journal of Physics D: Applied Physics **31**, 925 (1998).
[20] A. Fernández-Pacheco, D. Petit, R. Mansell, R. Lavrijsen, J. H. Lee, and R. P. Cowburn, Phys. Rev. B **86**, 104422 (2012).
[21] R. Lavrijsen, D. C. M. C. Petit, A. Fernández-Pacheco, J. Lee, R. Mansell, and R. P. Cowburn, Nanotechnology **25**, 105201 (2014).
[22] R. Mansell, D. C. M. C. Petit, A. Fernández-Pacheco, R. Lavrijsen, J. H. Lee, and R. P. Cowburn, Journal of Applied Physics **116**, 063906 (2014).
[23] S. Zhang, J. Zhang, A. A. Baker, S. Wang, G. Yu, and T. Hesjedal, Scientific Reports **4**, 6109 (2014).
[24] R. Moubah, F. Magnus, T. Warnatz, G. K. Palsson, V. Kapaklis, V. Ukleev, A. Devishvili, J. Palisaitis, P. O. A. Persson, and B. Hjörvarsson, Phys. Rev. Applied **5**, 044011 (2016).
[25] R. Lavrijsen, J. H. Lee, D. Petit, A. Fernández-Pacheco, R. Mansell, and R. P. Cowburn, Nature **493**, 647 (2013).
[26] J. Unguris, R. J. Celotta, and D. T. Pierce, Phys. Rev. Lett. **69**, 1125 (1992).
[27] D. Petit, R. Mansell, A. Fernández-Pacheco, J. Lee, and R. P. Cowburn, "Three-dimensional spintronics," in *VLSI: Circuits for Emerging Applications*, Devices, Circuits, and Systems, edited by T. Wojcicki (CRC Press, 2014) Chap. 12.
[28] A. Fernández-Pacheco, N.-J. Steinke, D. Mahendru, A. Welbourne, R. Mansell, S. L. Chin, D. Petit, J. Lee, R. Dalgliesh, S. Langridge, and R. P. Cowburn, Advanced Materials Interfaces **3**, 1600097 (2016), 1600097.
[29] D. Pierce, J. Unguris, R. Celotta, and M. Stiles, Journal of Magnetism and Magnetic Materials **200**, 290 (1999).
[30] S. Zohar, Y. Choi, D. M. Love, R. Mansell, C. H. W. Barnes, D. J. Keavney, and R. A. Rosenberg, Applied Physics Letters **106**, 072408 (2015).